INTERNATIONAL JOURNAL FOR NUMERICAL METHODS IN FLUIDS
Int. J. Numer. Meth. Fluids 2007; **53**:1–21
Published online 19 June 2006 in Wiley InterScience (www.interscience.wiley.com). DOI: 10.1002/fld.1239

Tracking accuracy of a semi-Lagrangian method for advection–dispersion modelling in rivers

S. Néelz*,† and S. G. Wallis

School of the Built Environment, Heriot-Watt University, Edinburgh EH14 4AS, U.K.

SUMMARY

There is an increasing need to improve the computational efficiency of river water quality models because: (1) Monte-Carlo-type multi-simulation methods, that return solutions with statistical distributions or confidence intervals, are becoming the norm, and (2) the systems modelled are increasingly large and complex. So far, most models are based on Eulerian numerical schemes for advection, but these do not meet the requirement of efficiency, being restricted to Courant numbers below unity. The alternative of using semi-Lagrangian methods, consisting of modelling advection by the method of characteristics, is free from any inherent Courant number restriction. However, it is subject to errors of tracking that result in potential phase errors in the solutions. The aim of this article is primarily to understand and estimate these tracking errors, assuming the use of a cell-based backward method of characteristics, and considering conditions that would prevail in practical applications in rivers. This is achieved separately for non-uniform flows and unsteady flows, either via theoretical considerations or using numerical experiments. The main conclusion is that, tracking errors are expected to be negligible in practical applications in both unsteady flows and non-uniform flows. Also, a very significant computational time saving compared to Eulerian schemes is achievable. Copyright © 2006 John Wiley & Sons, Ltd.

Received 9 November 2005; Revised 27 February 2006; Accepted 19 March 2006

KEY WORDS: Semi-Lagrangian; method of characteristics; pollutant transport; tracking errors; numerical efficiency

1. INTRODUCTION

In the last few decades, numerical modelling of environmental problems has greatly benefitted from the emergence of increasingly powerful computers. River hydrodynamics and mass transport scenarios can now be modelled using numerical schemes that are able to provide accurate solutions of the fully three-dimensional Navier–Stokes and advection–diffusion equations. However, the applicability of such 3D models to practical problems is challenged by the large quantity of

*Correspondence to: S. Néelz, School of the Built Environment, Heriot-Watt University, Edinburgh EH14 4AS, U.K.
†E-mail: s.p.f.neelz@hw.ac.uk

physical information required (channel geometry, turbulence parameters, friction parameters, turbulent diffusion coefficients), and the complicated form of the initial and boundary conditions [1]. Therefore, 2D and even 1D mathematical models are widely used in engineering practice. In the latter case, open-channel hydrodynamics are commonly modelled by the St-Venant equations, and mass transport is described by the advection–dispersion equation (see Reference [2]).

The advection–dispersion equation has sound physical foundations, and there is a considerable amount of evidence that it describes 1D mixing in many rivers reasonably well [3]. Also, its unidimensionality allows much faster numerical modelling than is permitted in the case of the 2D and 3D advection–diffusion equations. However, when combined with chemical or biological reactions, or with sediment sorption terms, the so-obtained river water quality model still relies on a number of parameters (dispersion coefficient, reaction coefficients, etc.), that are not generally known with sufficient accuracy. The effects of such uncertainties on model outcome can be assessed by using multi-simulation-based procedures such as the Monte-Carlo method [4]. This implies running the model a very large number of times, typically hundreds or thousands, depending on the number of parameters involved. This heavy computational cost emphasizes the need for increasingly efficient numerical methods, even in the current context of rapidly increasing computer power. This need is also motivated by the increase in the size and time scale of modelled environmental systems.

Traditional Eulerian numerical schemes (including finite-difference and finite-element methods) for advection–diffusion, on which most river water quality models are based, have a limited computational efficiency, because of limitations on the time step size that apply primarily to the advection solver, in the case of advection-dominated river flows (see References [5, 6]). These limitations are particularly clearly expressed for explicit schemes, where the condition for numerical stability is often that Cr, the Courant number ($Cr = U\Delta t/\Delta x$, where U is the velocity, and Δx and Δt are the space and time steps) should be smaller than 1.

The way forward towards the development of a numerical model for advection–dispersion that is not limited by Courant number restrictions is the Lagrangian approach, where the modelling of advection is based on the method of characteristics, which is faithful to the physical process of advection for all time step magnitudes. *Eulerian–Lagrangian* or *semi-Lagrangian* methods (Lagrangian methods that still rely on the use of a fixed computational grid) have been developed and advocated by various workers, either from a theoretical point of view or for various applications ranging from solute transport in porous media to ocean pollution studies and numerical weather prediction, see for example References [7–10]. However, these studies cannot be directly extended to the particular field of 1D solute transport in rivers, that, like any other, requires some specific physical scenarios to be considered. Such particular studies have been carried out by Manson and Wallis and co-workers (see for example References [6, 11–13]), who have demonstrated the potentially much superior computational efficiency of semi-Lagrangian methods (compared to Eulerian schemes) for advection–dispersion computations in steady uniform flows in rivers.

The purpose of this paper is to increase knowledge of the behaviour of semi-Lagrangian methods for advection–dispersion in one dimension by considering *non-uniform and unsteady river flows*. More specifically, this involves understanding the nature of and assessing the expected magnitude of the tracking errors that the method of characteristics may suffer from when applied to spatially and temporally varying flows. Also the potential for semi-Lagrangian methods to speed up 1D solute transport computations by at least one order of magnitude, compared to Eulerian methods, is considered. It is emphasized that the work is undertaken in light of the typical conditions that

DOI: 10.1002/fld

prevail in the context of river flows and river mass transport (of dissolved pollutant or even fine sediment) scenarios.

The paper starts, in Section 2, with a concise presentation of the advection–dispersion equation, followed by a demonstration of the limitations of Eulerian models for advection. Then the basic principles of semi-Lagrangian methods are introduced, including the approach more specifically used by the authors, the cell-based backward method of characteristics (referred to as CBMOC). In Section 3, tracking errors in non-uniform flows are approached from a theoretical point of view, being illustrated and quantified by a semi-theoretical test case. The case of unsteady flows is then studied by numerical experiments in Section 4. The issue of computational time is considered in Section 5.

2. BACKGROUND

2.1. The 1D advection–dispersion equation in non-uniform unsteady flows

The cross-sectional averaged 1D advection–dispersion equation for mass transport in unsteady non-uniform incompressible flows reads:

$$\frac{\partial C}{\partial t} + U\frac{\partial C}{\partial x} = \frac{1}{A}\frac{\partial}{\partial x}\left(AD\frac{\partial C}{\partial x}\right) \tag{1}$$

where C, U and A are the cross-sectional averaged concentration and velocity, and the cross-sectional area, respectively. The dispersion process (RHS term) arises from the combined effects of longitudinal spreading due to transverse and vertical velocity gradients (velocity shear), and transverse and vertical mixing. It was shown by Fischer [14] and Fischer *et al.* [2] that dispersion could be described by a diffusion equation provided that turbulence is stationary and homogeneous and that sufficient time has elapsed since the solute entered the flow. The coefficient D is the so-called *dispersion* coefficient. It has been estimated in numerous rivers, with a very wide variation in the reported values, from 1 to 10^3 m^2 s^{-1} (see for example References [3, 15]).

2.2. Limitations of Eulerian schemes

A forward in time, central in space, finite difference interpretation of the 1D pure advection equation, i.e. Equation (1) with $D = 0$, reads:

$$\frac{C_i^{n+1} - C_i^n}{\Delta t} + U\frac{C_{i+1/2}^n - C_{i-1/2}^n}{\Delta x} = 0 \tag{2}$$

where $C_{i-1/2}^n$ and $C_{i+1/2}^n$ are, respectively, the left- and right-hand side wall values of C for the ith computational cell. These wall values are interpolated from adjacent nodal values in some way, resulting in well-known explicit schemes [16], such as the upwind scheme, the central scheme, or the QUICK scheme (see Reference [17]).

The use of any of these schemes faces a major restriction originating in the fact that under many conditions the *numerical* region of influence, or the ensemble of node concentrations at time level n on which the concentration C_i^{n+1} depends in the numerical scheme, and the real or *physical* region of influence, are distinct. In other words, the CFL condition [18] is not satisfied. The CFL

DOI: 10.1002/fld

condition is a necessary, but not sufficient, condition for accuracy. It usually takes the form $Cr \leqslant 1$ for explicit Eulerian schemes.

An additional drawback of explicit Eulerian advection schemes is that they are unstable when not meeting the CFL condition. It is well-known that some schemes (for example, QUICK, central) are even unconditionally unstable, while the upwind scheme, as well as other explicit schemes such as the Lax scheme, the Staggered Leapfrog scheme, or the Lax–Wendroff scheme are subject to the stability condition expressed by $Cr \leqslant 1$. An update on stability conditions of explicit schemes has been proposed by Leonard [19].

Implicit schemes represent an effective way to circumvent stability problems. However, their structure is still such that C_i^{n+1} depends primarily on the concentrations at a small number of neighbouring nodes, and therefore they are not accurate at much higher Courant numbers than those permitted on stability grounds in explicit schemes (see for example References [5, 6]).

Finally, it should be added that while the Courant number restriction may be eased as a result of the effect of physical diffusion, this is at the expense of severe restrictions on the cell-Péclet number Pe ($Pe = U\Delta x/D$) that prove to be impractical in applications to rivers, which are usually advection-dominated.

In conclusion, finite-difference schemes for advection have a limited potential in terms of computational efficiency, because of the restriction that the Courant number cannot normally exceed the order of 1. A similar state of affairs also applies to other Eulerian methods such as the finite-element method.

2.3. Semi-Lagrangian models

Lagrangian methods have a very palpable physical interpretation since they simply consist in tracing trajectories, understood as the curves $x = x(t)$ that are followed by pollutant particles, described by

$$\frac{\mathrm{d}x}{\mathrm{d}t} = U(x, t) \tag{3}$$

Such curves are called *characteristic lines* or, simply, *characteristics*. The pure advection equation is equivalent to the statement

$$\frac{\mathrm{d}C}{\mathrm{d}t} = 0 \tag{4}$$

as long as this is evaluated along a characteristic line. In other words, the *substantial derivative* of the concentration is zero, as far as pure advection is concerned.

The process of tracing a characteristic line backwards from the arrival node $(x_i, (n+1)\Delta t)$ to the departure point $(x_\xi, n\Delta t)$, or *foot* of the characteristic line, is referred to as characteristic *tracking*. It is done by integrating Equation (3) as follows:

$$x_\xi = x_i + \int_{(n+1)\Delta t}^{n\Delta t} U(x(\tau), \tau)\, \mathrm{d}\tau \tag{5}$$

where τ is a dummy integration variable. It is then evident that

$$C_i^{n+1} = C_\xi^n \tag{6}$$

DOI: 10.1002/fld

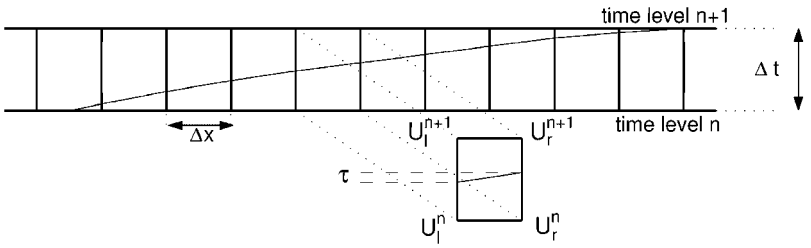

Figure 1. Cell-wise linear characteristic lines in 1D.

The value of C_{ξ}^{n} must be interpolated from the known nodal values of the concentration at time level n.

Semi-Lagrangian methods are in perfect accord with the physical process of advection, regardless of the Courant number. However, their accuracy is still subject to three main issues, namely (1) tracking of the characteristics, (2) departure point interpolation and (3) the potential absence of perfect mass conservation.

In the majority of publications on semi-Lagrangian methods, characteristic tracking is based on integration procedures such as Runge–Kutta methods (the second-order RK method is used in, for example, References [20–23], the fourth-order RK method is used in, for example, References [24, 25]). This normally involves a tracking substep δt ($=\Delta t/N$, where N is an integer), the size of which depends on the flow variability. In many studies concerned with rapidly varying flow scenarios, it is found that δt must be such that the corresponding (δt-based) Courant number cannot normally exceed 1, for accuracy reasons. An additional limitation of RK methods is that the process of interpolating the required velocity values at the intermediate points of the tracking procedure is expensive in terms of computational cost [24], even though a low-order interpolation scheme is generally sufficient [8].

A minority of published schemes have used a simplified tracking technique, where characteristic lines are cell-wise linear, as in Figure 1. Here, in each cell, a unique average value of the velocity is used to compute the slope of all the characteristic lines crossing the cell. This method has a significant advantage over RK methods in terms of efficiency: the cell-increments (or travel times) τ need to be calculated once only for each cell (for each time step), whereafter they can be stored and used for each characteristic line crossing the cell.[‡] This is the approach used by Roache [7], Wallis and Manson [13] and Manson and Wallis [11, 12], in the context of their DISCUS method, and in the present paper. A simple expression for the cell-averaged velocity $\overline{U}$ (used to compute $\tau=\Delta x/\overline{U}$) was proposed by Roache [7]:

$$\overline{U}=\frac{U_{\mathrm{l}}^{n}+U_{\mathrm{r}}^{n}+U_{\mathrm{l}}^{n+1}+U_{\mathrm{r}}^{n+1}}{4} \tag{7}$$

where U_{l}^{n}, U_{r}^{n}, U_{l}^{n+1} and U_{r}^{n+1} refer to the values of the velocity at the four corners of the cell as shown in Figure 1. To date, no systematic assessment of the tracking accuracy of this method in either non-uniform or unsteady flow has been published.

[‡]They are recalculated at every time step, unless the flow is steady.

DOI: 10.1002/fld

Interpolation of concentrations at the departure points is recognized to cause errors particularly when concentration profiles exhibit narrow extrema and discontinuities. This is also a strongly case-dependent issue and, while a large number of interpolators have been developed, none of them can be recognized as being optimal [8, 9]. While linear interpolation is overwhelmingly rejected on the grounds that it causes excessive numerical diffusion [26], second-order (quadratic) polynomial interpolation suffers from asymmetry leading to potential phase errors [27, 28]. However, third-order (cubic) polynomial interpolation has been frequently used [11], although this scheme (and any other higher-order polynomial scheme) is liable to cause unphysical oscillations in the event of narrow extrema and discontinuities. Wallis and Manson [13] have been able to suppress these oscillations using a flux limiter and a flux-based version of this interpolation scheme, albeit at the expense of some loss in accuracy. Spline interpolators have been advocated in, for example, References [21, 23, 29, 30]. Neuman [31] proposed an adaptive scheme where forward-tracked clustered particles would locally improve spatial resolution around sharp fronts. Néelz [32] concluded that cubic polynomial interpolation was satisfactory in most cases of pollutant transport in rivers.

The possible non-conservative behaviour of semi-Lagrangian schemes [33] has been more extensively addressed in the context of finite-element methods (FEM), leading to schemes such as Eulerian–Lagrangian localized adjoint method (ELLAM), see Reference [10], which are inherently mass-conservative. A systematic study of the conservativeness of a number of FEM-based schemes can be found in Reference [34]. Interestingly, some conservative finite-difference-based semi-Lagrangian schemes have been proposed, for example in References [11, 12], where use is made of the cumulative mass profile, $M(x)$, instead of the concentration profile, $C(x)$, where $M(x)$ is defined as

$$M(x) = \int_0^x C(x)A(x)\,\mathrm{d}x \tag{8}$$

Other approaches have been introduced by Burguete and Garcia-Navarro [35], and Zoppou and Roberts [36]. The lack of exact mass conservation has not been found to be a serious problem in practical applications such as numerical weather prediction [8], or pollutant transport in rivers [32].

Boundary conditions are usually handled by interpolating departure concentration values on the time axis at $x = 0$ instead of on the space axis. Interpolation accuracy will follow a similar behaviour as for initial conditions and, therefore, do not require special attention. However, the calculation of diffusion during the initial time step will need to involve a reduced diffusion time to take into account the non-zero departure times at the feet of the characteristics. This is detailed in Reference [32].

3. APPLICATION TO STEADY NON-UNIFORM RIVER FLOWS

In (steady) uniform flows, the velocity is a constant. Every characteristic line is a straight line and the only type of error involved in the semi-Lagrangian modelling of advection is the concentration interpolation error, introduced in Section 2.3. However, steady uniform flow modelling is of limited interest, as most river flows feature variations, at least in space, i.e. they are non-uniform.

Non-uniform, yet steady, flows, are considered in this section. In unsteady flows, the unsteadiness induces some non-uniformity (unsteady flows are always non-uniform), and thereby non-uniformity errors, but this type of error is covered in Section 4.

DOI: 10.1002/fld

3.1. Theory

In steady non-uniform flows, Equation (7) reverts to

$$\overline{U} = \frac{U_\mathrm{l} + U_\mathrm{r}}{2} \tag{9}$$

which is consistent with:

$$\tau = \frac{2\Delta x}{U_\mathrm{l} + U_\mathrm{r}} \tag{10}$$

The exact nature of the approximations made (in the process of tracking the characteristic line) when using Equations (9) and (10) can be understood by the following considerations.

In steady non-uniform flows, the values of the velocity at the nodes, U_i, are different from node to node (although constant in time). From a theoretical point of view, τ should be evaluated by first assuming a function $U(x)$ describing the velocity across a cell, from $x = x_\mathrm{l}$ at the left-hand node to $x = x_\mathrm{r}$ at the right-hand node (see Figure 2), and then performing the following integration:

$$\tau = \int_{x_\mathrm{l}}^{x_\mathrm{r}} \frac{1}{U(x)}\,\mathrm{d}x \tag{11}$$

As t_r is known from the calculations conducted in association with the adjoining cell on the right-hand side, the value of t_l is simply $t_\mathrm{l} = t_\mathrm{r} - \tau$. Repeated application of this idea enables the characteristic to be tracked in a cell-wise manner.

The choice of $U(x)$ is effectively an interpolation problem. For example, if a cubic spline or a cubic polynomial interpolation is used, $U(x)$ becomes a third-order polynomial, and the integration of Equation (11) can in principle be performed analytically. However, this involves a rather complicated combination of polynomials, *ln* and *arctan* functions, potentially implying a large computational cost, repeated for every cell. It is not clear whether the increased accuracy is worth the computation time involved. Consequently, it is worth testing the much simpler alternative of Equation (10).

Using Equation (10) could be seen as consistent with assuming a linear internode variation of $U(x)$. In fact this is not exactly the case, as shown by the following. The assumption of linear internode variation between the node values $U(x_\mathrm{l}) = U_\mathrm{l}$ and $U(x_\mathrm{r}) = U_\mathrm{r}$ implies that

$$U(x) = U_\mathrm{l} + \frac{x - x_\mathrm{l}}{x_\mathrm{r} - x_\mathrm{l}}(U_\mathrm{r} - U_\mathrm{l}) \quad \text{for } x_\mathrm{l} \leqslant x \leqslant x_\mathrm{r} \tag{12}$$

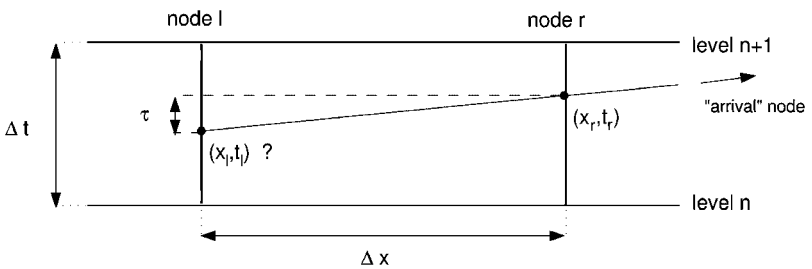

Figure 2. Definition of the cell (or internode) travel time τ, and of the points $(x_\mathrm{l}, t_\mathrm{l})$ and $(x_\mathrm{r}, t_\mathrm{r})$.

DOI: 10.1002/fld

Combining Equations (11) and (12), integrating and recalling that $x_r - x_l = \Delta x$ yields:

$$\tau = \Delta x \frac{\ln(U_r) - \ln(U_l)}{U_r - U_l} \quad \text{if } U_l \neq U_r \tag{13}$$

or

$$\tau = \frac{\Delta x}{U_l} \quad \text{if } U_l = U_r \tag{14}$$

Equations (13) and (14) provide the exact value of τ if a linear variation of $U(x)$ is assumed. In contrast, Equation (10) provides an approximation of Equations (13) and (14).

Introducing τ_{linear} as the value of τ calculated by Equation (13) (or (14)) and τ_{approx} as its value calculated by Equation (10), it can be shown that $0.999 \leqslant \tau_{approx}/\tau_{linear} \leqslant 1$ provided that $0.9 \leqslant U_r/U_l \leqslant 1.1$. In other words, τ_{approx} provides an excellent approximate value of τ_{linear} if the velocity variation across the cell is less than 10%. However, if the velocity variation is larger than 10%, τ_{approx} may be significantly smaller than τ_{linear}. It is worth adding that it is never larger ($\tau_{approx}/\tau_{linear} \leqslant 1$ for any value of U_r/U_l), which implies that the errors occurring along the channel *add up*, and never cancel each other.

3.2. Example and results

The example proposed here features a channel where the velocity $U(x)$ varies with distance according to a Gaussian, as in

$$U(x) = \exp\left(-\frac{(x - x_U)^2}{2\sigma_U^2}\right) \cdot \Delta U + U_0 \tag{15}$$

where x_U is the abscissa of the centroid of the velocity profile, σ_U is its standard deviation, U_0 is the 'base' value of the velocity (its value outside the Gaussian profile), and ΔU is the amplitude of the velocity variation. With $x_U = 15\,000$ m, $\sigma_U = 250$ m, $U_0 = 1\ \mathrm{m\,s^{-1}}$ and $\Delta U = 4\ \mathrm{m\,s^{-1}}$, the velocity profile is as shown in Figure 3(a). In the context of real rivers, such a velocity variation can be considered severe, yet physically realistic.

Using a cell length, Δx, equal to 100 m, the following quantities were evaluated:

- τ_{exact} using Equation (11) and the $U(x)$ function from Equation (15),[§]
- τ_{linear} using Equations (13) or (14), and the node values U_l and U_r, calculated using the same Equation (15),
- τ_{approx} using Equation (10) and the same values of U_l and U_r,
- ε_{linear} defined as $\varepsilon_{linear} = \tau_{linear} - \tau_{exact}$,
- ε_{approx} defined as $\varepsilon_{approx} = \tau_{approx} - \tau_{linear}$,
- ε_{total} defined as $\varepsilon_{total} = \tau_{approx} - \tau_{exact} = \varepsilon_{linear} + \varepsilon_{approx}$.

The quantity ε_{linear} is the error (in the value of τ) due to the internode linearity assumption. The quantity ε_{approx} is the additional error due to the use of Equation (10) instead of

[§]This was done numerically, within a relative error of 10^{-3}, using an adaptive recursive Simpson's rule (preprogrammed function in MATLAB).

DOI: 10.1002/fld

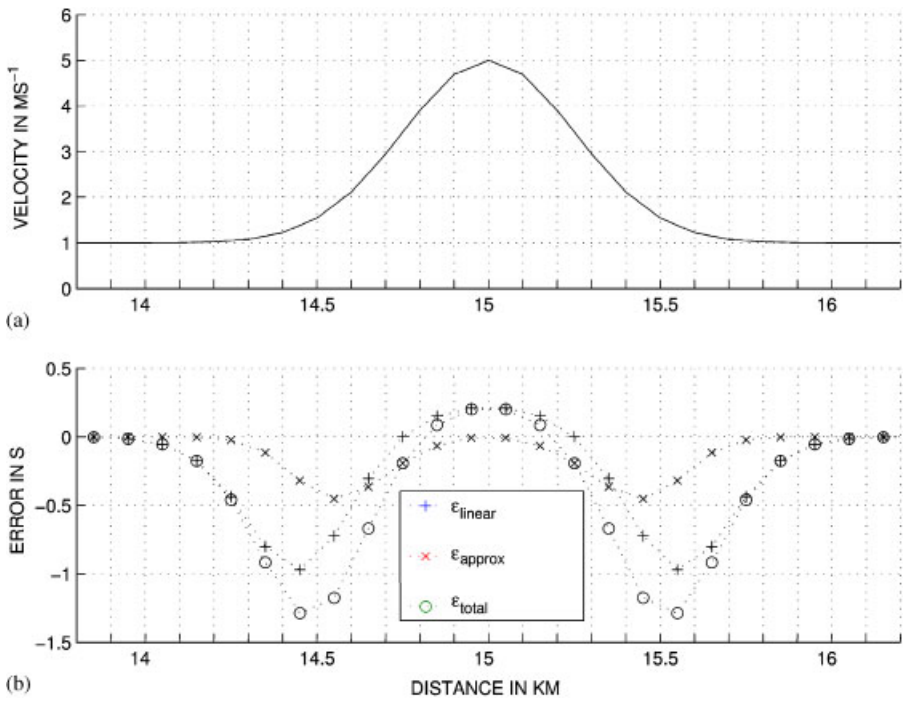

Figure 3. (a) Velocity profile; and (b) values $\varepsilon_{\text{linear}}$, $\varepsilon_{\text{approx}}$, and $\varepsilon_{\text{total}}$. The vertical lines show the locations of the spatial nodes.

Equation (13). The quantity $\varepsilon_{\text{total}}$ is the sum of these errors, i.e. the total error due to the use of Equation (10), instead of a supposedly exact method.

Figure 3(b) shows the values of $\varepsilon_{\text{linear}}$, $\varepsilon_{\text{approx}}$, and $\varepsilon_{\text{total}}$ in all the cells affected by the velocity variation. The first observations that can be made are that $\varepsilon_{\text{linear}}$ and $\varepsilon_{\text{approx}}$ depend on the variations of U in a manner that is consistent with most expectations, with $\varepsilon_{\text{approx}}$ being largest where the first gradient of $U(x)$ is largest, and $\varepsilon_{\text{linear}}$ being largest (in absolute value) where the second and higher order gradients of $U(x)$ are largest. However, it should also be noted that $\varepsilon_{\text{linear}}$ is not very large in the part of the channel corresponding to the peak of the Gaussian profile, despite the presence of large second and higher order gradients of $U(x)$. This is due to the high velocity there, that induces a small internode travel time τ, and hence a small absolute error in τ. This feature may not be specific to the present example, as, in general, convexities in the upward and downward direction are found more in conjunction with regions of higher and lower velocities, respectively. Therefore, $\varepsilon_{\text{linear}}$ would, in general, take greater negative values than positive ones.

A characteristic line tracked down from the 'arrival' point at time-level $n+1$, through this non-uniform flow, and down to the 'departure' point at time-level n is subject to the total error:

$$E_{\text{total}} = E_{\text{linear}} + E_{\text{approx}} = \sum \varepsilon_{\text{total}} \tag{16}$$

DOI: 10.1002/fld

where

$$E_{\text{linear}} = \sum \varepsilon_{\text{linear}} \tag{17}$$

and

$$E_{\text{approx}} = \sum \varepsilon_{\text{approx}} \tag{18}$$

where the summations are performed over all the cells through which the characteristic passes.

In the present example, let us assume that the characteristic passes through all the cells represented in Figure 3. The total errors are reported in column one of Table I.

If one wishes to improve the accuracy of the solute transport simulation in this case, one obvious method consists of reducing the cell length Δx, so as to improve spatial resolution. It can be verified in columns two and three of Table I, that if spatial resolution is increased by a factor of 2 and 4, E_{total} is reduced by a factor of 3.9 and 15.8, respectively. Also, column four shows that if spatial resolution is worsened by a factor of 2, E_{total} is increased by a factor of 3.8. These results clearly indicate a second-order dependence of model accuracy on grid resolution. It is also interesting to test different cases, featuring a more gradual velocity variation over a longer distance. To this end, σ_U was increased by a of factor 2 and 4. Columns five and six show that, as a result, accuracy was improved by a factor of 2.0 and 3.9, respectively. With σ_U reduced by a factor of 2, accuracy was worsened by a factor of 1.9 (column seven). Finally, cases with a smaller velocity amplitude were tested. With ΔU reduced by a factor of 2 and 4, accuracy was improved by a factor of 1.7 and 3.4 (columns eight and nine), respectively. With ΔU increased two-fold, E_{total} was increased by a factor of 1.4 (column 10). These results suggest clearly a first-order dependence of E^{total} on σ_U, possibly also on ΔU.

E_{total} represents a vertical shift of the left-hand end of a characteristic line. It translates into a sideways shift of the departure point (tracking error), and consequently into a phase error in the concentrations at time-level $n+1$. The magnitude of this phase error (a distance) depends on the velocity in the vicinity of the departure point.

With a velocity at the foot of the characteristic line equal to $1\ \text{m s}^{-1}$ in this example, and $E_{\text{total}} = -9.31$ s as in column one in Table I, the phase error is consequently $+9.31$ m after the solute has passed through the zone of variation. The effect of this on the accuracy of concentration values depends on the size and shape of the concentration profile. It can be shown [32] that for a poorly resolved Gaussian concentration profile of dimensionless standard deviation $\Sigma = 4$ (or standard deviation $\sigma = \Delta x \cdot \Sigma = 400$ m), the error does not exceed 5% in the central part of the profile where $C \geqslant C_{\text{peak}}/10$. If Σ becomes greater than 4 due to the effect of diffusion, this error

Table I. Cumulative errors (absolute values).

Case	1	2	3	4	5	6	7	8	9	10
Δx (m)	100	50	25	200	100	100	100	100	100	100
ΔU (m s^{-1})	4	4	4	4	4	4	4	2	1	8
σ_U (m)	250	250	250	250	500	1000	125	250	250	250
E_{linear} (s)	6.23	1.57	0.40	23.98	3.15	1.58	11.99	3.74	1.85	8.93
E_{approx} (s)	3.08	0.78	0.20	11.49	1.57	0.79	5.74	1.86	0.92	4.37
E_{total} (s)	9.31	2.36	0.59	35.47	4.72	2.37	17.73	5.60	2.77	13.30

Cases 1–10 are described in the text. All the errors were found to be negative.

DOI: 10.1002/fld

can be reduced more, potentially to less than 1%. With a smaller value of Δx, it can be made even smaller.

3.3. Discussion

The first issue that is brought to light by the example studied above is the tendency of $\varepsilon_{\text{linear}}$ to take greater negative than positive values. Bearing in mind the fact that $\varepsilon_{\text{approx}}$, is *always* negative, the total travel time error E_{total} is therefore most likely to be negative. This results in the movement of the solute by advection to be modelled faster than it should be. However, the calculated phase error of +9.31 m is moderate, despite the very severe non-uniformity of $U(x)$. The impact on the overall model accuracy depends on the size of the solute 'cloud' compared to the phase shift. It is unlikely to be significant in practical applications.

The likelihood of a velocity variation of this shape and amplitude occurring (from 1 to $5\,\text{m}\,\text{s}^{-1}$, and back to $1\,\text{m}\,\text{s}^{-1}$, within a total distance of 2000 m) is a matter for discussion, but an even more important issue is the likelihood of it being repeated many times over the length of a river. In extremely non-uniform rivers, a total tracking error reaching values of up to, say, hundreds of meters should not be considered unrealistic, but the example above also shows that an efficient way to reduce it consists of reducing Δx, since it depends on Δx with a second-order dependency.

These conclusions should also be viewed in the context of open channel flow modelling. Any flow model used to generate the flow field used in a pollutant transport simulation is subject to errors that may take on significant proportions, mainly because of the lack of accuracy of the data related to the river geomorphology. A clear example is the roughness coefficient involved in the modelling of bed friction. One of the most widely used, Manning's n,[¶] is commonly chosen between ~ 0.02 for a clean straight lowland stream and ~ 0.1 for an irregular and rough river (see for example Reference [1]). An error in the value of n causes errors in U of similar proportions, and therefore would result in potentially large errors in the results of a flow model. Additionally, the advection–dispersion equation, Equation (1), is only valid in theory if a number of assumptions are met, including that turbulence is stationary and homogeneous. There is some controversy about its use in rivers that are significantly different from the ideal case of a uniform channel of constant depth (see References [37, 38]). These comments put into context the limited relevance of seeking an excessively high tracking accuracy in any model of advection–dispersion in rivers.

4. APPLICATION TO UNSTEADY RIVER FLOWS

In this section, we assume that the velocity varies in time, which also implies that it varies in space, since variations in time only are physically unrealistic. Unsteady flows are highly relevant to fluvial water quality problems, because concerns about pollution often occur in conjunction with varying flows, for example when water levels reach unusual values during floods.

4.1. River flow modelling

The modelling of river hydrodynamics is outwith the scope of this paper. It is also emphasized that there is no coupling between the flow and the transport, since the flow is assumed not to be affected by the transport processes. This is a valid assumption in all practical cases of pollutant

[¶] It is recalled that $U = R^{2/3} S_f^{1/2}/n$, where R is the hydraulic radius, and S_f is the energy slope.

DOI: 10.1002/fld

transport in rivers. Also, it is an underlying assumption of this work concerning mass transport, that the flow field is computed prior to the transport model being applied. This is assumed to be done using the same discretization in space, whereas the time step in the flow model, denoted Δt_{CFD}, will depend on the computational fluid dynamics (CFD) method used, and is not expected to be the same as Δt_{T}, the one used eventually in the transport model. The value of Δt_{CFD} has a significant bearing on the accuracy of the transport model in unsteady flows, because it determines the time-resolution with which the hydrodynamic data, on which the transport modelling relies, are available.

Channel flow is normally modelled using the well-known *shallow water* or *St-Venant* equations for cross-sectionally averaged gradually varied unsteady flow. In river studies, these are solved using various numerical methods including methods of characteristics, Riemann solvers, finite elements and finite differences (FD). An increasing number of research codes have been based on shock-capturing schemes such as explicit Riemann solvers but in practice implicit FD schemes predominate, particularly in commercial software. These can be used with large Courant numbers, typically up to 10 or 20. However, they do not provide accurate results with $Cr \gg 1$ in highly unsteady flows [39], where flood waves must be described with a sufficient time-resolution. For this reason, it is assumed in this article that Δt_{CFD} is chosen as large as possible, although such that $Cr(\mathit{flow})$ does not exceed the order of 1.

4.2. Details of method used for characteristic tracking

It is assumed that the time step used in the transport model, Δt_{T}, is much larger than Δt_{CFD}, because the ambition of the present work is to allow $Cr \gg 1$ in the transport model, as introduced earlier.

Assuming, as before, that a cell-based method of characteristics (CBMOC) is used, let us consider the task of tracking a characteristic line backward from the 'arrival' node, at time-level $n+1$, to the 'departure' point, or foot, at abscissa x_ξ and time-level n. The flow is unsteady, so that at any node j, we have in general $U_j^{n+1} \neq U_j^n$. In each cell, the travel time $\tau = t_{\mathrm{r}} - t_{\mathrm{l}}$ (see Figure 2) is now defined as follows:

$$\tau = \int_{x_{\mathrm{l}}}^{x_{\mathrm{r}}} \frac{1}{U(x,t)}\,\mathrm{d}x \tag{19}$$

which involves the additional dependence of U on t. This is less straighforward to evaluate than Equation (11). However, it is mathematically equivalent to solving the following differential equation:

$$\frac{\mathrm{d}t(x)}{\mathrm{d}x} = f(x,t) \tag{20}$$

where $f(x,t) = 1/U(x,t)$, with the initial condition $t(x_{\mathrm{r}}) = t_{\mathrm{r}}$.

Such an equation can be solved numerically, for $t(x_{\mathrm{l}}) = t_{\mathrm{l}}$, by, for example, Runge–Kutta methods. Discussing the accuracy and the computational efficiency of such methods is beyond the scope of this article. However, these will entail computational efficiency issues, as the same procedure has to be applied in every cell, for every characteristic line, and repeated at every time step.

DOI: 10.1002/fld

Runge–Kutta methods are not considered any further in this paper. Instead, it is proposed to use a much simpler method based on Equation (7). This is expected to be accurate enough in river applications, where the unsteadiness-related variation of U across the cells, both in time and space, is of limited magnitude.

As mentioned earlier, Δt_{CFD} is assumed to be many times smaller than the time step used in the transport model, Δt_{T}. As a consequence, a characteristic line tracked from the arrival point at the time level $n+1$, down to the departure point at time level n, intersects many time levels of the flow computation. In the proposed CBMOC method, the characteristic line is piecewise linear, with a linear segment in each cell delimited by two nodes and two flow time-levels, and Equation (7) is applied in turn to each of these segments, as follows:

$$\tau = \frac{4\Delta x}{U_{\mathrm{l}}^{v} + U_{\mathrm{r}}^{v} + U_{\mathrm{l}}^{v+1} + U_{\mathrm{r}}^{v+1}} \tag{21}$$

where l and r refer to, respectively, the left- and right-hand node, while v and $v+1$ refer to the previous and the next time-levels in the flow model. For reasons of simplicity, it is assumed that $\Delta t_{\mathrm{T}}/\Delta t_{\mathrm{CFD}}$ is an integer, so that the transport time-levels coincide with flow time-levels. The CBMOC is illustrated in Figure 4.

Equation (21) can be seen as an extension of Equation (10) to unsteady flows (and it reverts to Equation (10) if the flow is steady). It provides an approximate value of the cell travel time within each cell, in which the average velocity $\overline{U} = \Delta x/\tau = (U_{\mathrm{l}}^{v} + U_{\mathrm{r}}^{v} + U_{\mathrm{l}}^{v+1} + U_{\mathrm{r}}^{v+1})/4$ is used to compute the slope of the characteristic curve, independently of the values of t_{l} and t_{r}.

4.3. Example

The CBMOC was tested for a case of pure advection in a channel subjected to a rather sudden velocity increase, where it is expected that significant unsteadiness-related tracking errors are the most likely to appear in the semi-Lagrangian modelling. These errors are expected to depend on the cell length Δx, the order of magnitude of the velocity, the amplitude of the velocity variations, the velocity gradients, the time step used in the flow model, the time step used in the solute transport model and the number of time steps calculated.

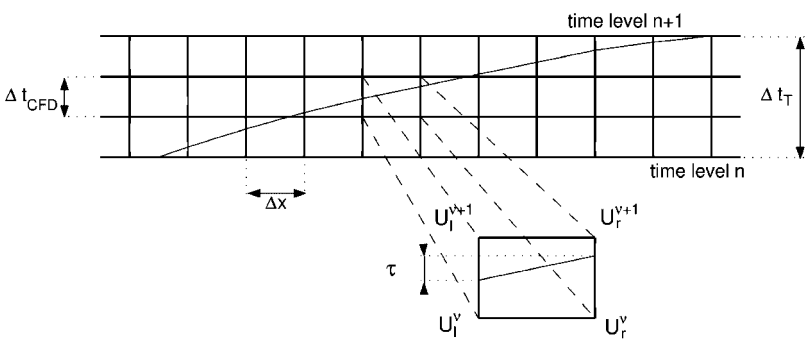

Figure 4. Illustration of the CBMOC ($\Delta t_{\mathrm{T}}/\Delta t_{\mathrm{CFD}} = 3$ in this figure).

DOI: 10.1002/fld

The test concerned a channel where the velocity was as specified by the following equation:

$$U(x,t) = -\tanh\left(\frac{x - x_0 - c \cdot t}{10^3 \cdot d(t)}\right) \cdot \frac{(U_{\max} - U_{\min})}{2} + \frac{U_{\max} + U_{\min}}{2} \tag{22}$$

This describes a wave front travelling down the channel, with x_0 being the position of the wave front centre of symmetry at time $t = 0$, c being the wave celerity, $d(t)$ being an empirical 'slope' factor varying with time and representing the longitudinal spreading of the wave, $U_{\max}$ being the water velocity upstream of the wave and $U_{\min}$ being the water velocity downstream of the wave. Using Equation (22) with $U_{\min} = 1.43\,\mathrm{m\,s^{-1}}$, $U_{\max} = 2.14\,\mathrm{m\,s^{-1}}$, $c = 2.54\,\mathrm{m\,s^{-1}}$, $x_0 = 333\,\mathrm{m}$, and $d(t) = 0.6 + 0.9 \cdot t/3600$, the velocity field in the first 24 km and for the first 2.5 h is as shown in Figure 5(a). Under these conditions, any pollutant already present in the channel before the occurrence of this wave is at some point submitted to rapid velocity variations. It is emphasized that the wave front travels faster than the flow and that the velocity remains equal to $U_{\max}$ in the wake of the wave.

Equation (22) was not chosen in an arbitrary manner. It was derived to closely fit the evolution of the velocity profile as computed using a river modelling software package (ISIS Flow), in a channel with a bottom slope of 0.2%, and a V-shaped cross-section with side slopes of 45° from the horizontal. Manning's roughness coefficient was set to 0.03. The discharge was initially (time $t = 0$) $10\,\mathrm{m^3\,s^{-1}}$ along the entire channel. From $t = 120$ to 600 s, the discharge at the upstream boundary was increased linearly from 10 to $50\,\mathrm{m^3\,s^{-1}}$. It was thereafter kept constant at $50\,\mathrm{m^3\,s^{-1}}$. The time step used in the ISIS Flow calculations was 120 s.[‖]

Tracking errors in the transport model using the CBMOC were investigated experimentally in the following way:

1. The outcome of the computation of the flow field was simulated by sampling nodal velocities using Equation (22) at a resolution in time defined by Δt_{CFD}, the time step assumedly used in the flow computation.
2. The solutions of an initial condition transport problem (detailed below) using the CBMOC with increasingly long time steps were computed, using the discrete nodal velocities computed in 1.
3. These solutions were compared to 'exact' benchmark solutions of the same problem, obtained using the continuous (non-discrete) velocity field provided by Equation (22),[**] an iterative Runge–Kutta technique[††] to integrate Equation (5), and a fifth-order polynomial interpolation scheme at the foot of the characteristic lines tracked down from every time-level to $t = 0$.

The results from three cases numbered 1, 2, 3, are presented here. Cases 2 and 3 are similar to Case 1, but with different values of Δx and Δt_{CFD}. Case 1 is introduced first.

[‖]This was the largest that could be used to resolve the inflow boundary condition properly, but was also approximately the largest that ensured a good accuracy of the CFD scheme used in the software, the Courant number taking values up to 2.6.

[**]Not the velocity field in its discrete form provided by ISIS.

[††]Based on an explicit Runge–Kutta formula, the Dormand–Prince pair; relative error tolerance 10^{-3} and absolute error tolerance 10^{-6} obtained by iteration (preprogrammed function in MATLAB).

DOI: 10.1002/fld

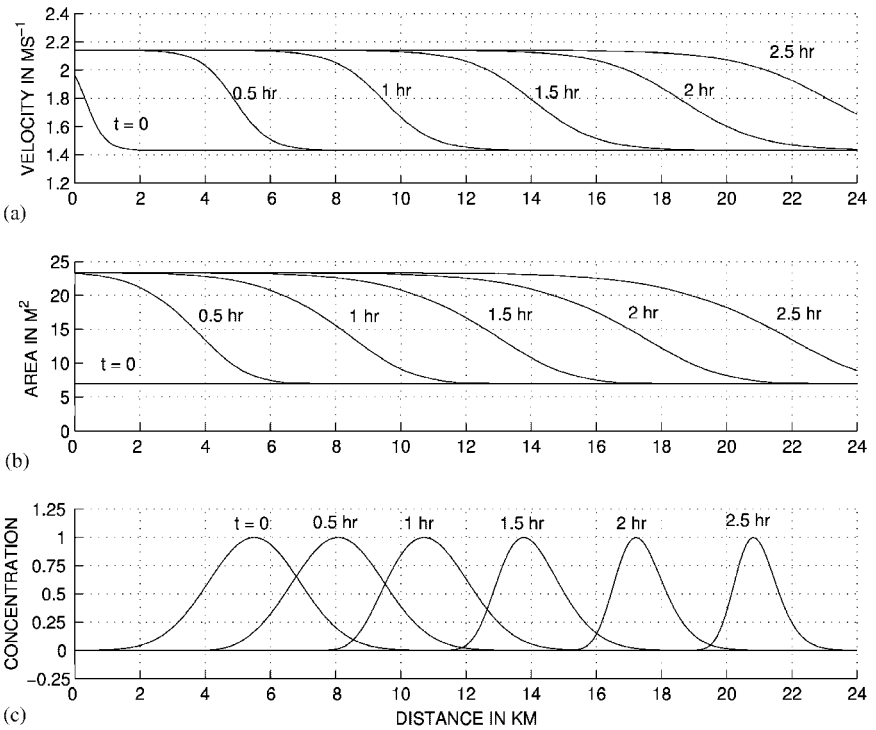

Figure 5. Evolution in time and space, represented every half hour, of: (a) flow velocity; (b) flow cross-sectional area; and (c) normalized (benchmark) solute concentration ($=c/c_{\text{peak}}$ where c_{peak} is the initial peak concentration).

In Case 1, the cell size Δx was 100 m. The initial condition of the solute transport problem consisted of a Gaussian profile of initial dimensionless standard deviation $\Sigma = 14$ ($\sigma = 14 \cdot \Delta x$), centred at a location 5500 m from the upstream boundary at time $t = 0$. The CBMOC was used with a fifth-order polynomial interpolation scheme for evaluating concentration at the foot of the characteristic. This ensured an excellent interpolation accuracy all the way through the test.[‡‡]

The time resolution of the flow data was $\Delta t_{\text{CFD}} = 120$ s. The time step used in the semi-Lagrangian transport model Δt_{T} was made increasingly large, always such that $\Delta t_{\text{T}}/\Delta t_{\text{CFD}}$ was an integer, starting with $\Delta t_{\text{T}} = \Delta t_{\text{CFD}}$.

The evolution in time of the benchmark spatial solute concentration profile is shown in Figure 5(c), and should be viewed in conjunction with the corresponding velocity and flow cross-sectional area results shown in Figures 5(a) and (b), respectively.

Cases 2 and 3 were similar to Case 1, although with different parameter values as detailed in Table II.[§§] Cases 2 and 3 are useful to the understanding of the effects of reducing the cell size Δx and the flow computation time step Δt_{CFD}, respectively.

[‡‡]The present tests, concerned with tracking errors, needed to be free from any noise caused by interpolation errors. Such a high level of interpolation accuracy would not be required in practice.

[§§]Consistently, $\Sigma = 28$ in Case 2 instead of 14, so that the initial solute profile keeps the same size as in Cases 1 and 3.

DOI: 10.1002/fld

Table II. Values of Δx and Δt_{CFD} used in Cases 1–3.

	Case 1	Case 2	Case 3
Δx (m)	100	50	100
Δt_{CFD} (s)	120	120	60

4.4. Results

The numerical solute concentration results were not visually distinguishable from the benchmark solutions presented in Figure 5(c), for any of the three cases and for any of the time steps used. Mass conservation was checked and any change in total mass was always small, being no greater than 3%. It is noted that the apparent reduction in size of the concentration profile in Figure 5(c) does not indicate a loss of mass, because the cross-sectional area of the flow increases with increasing velocity as shown by Figure 5(b).

The evolution in time of the phase error at the centre of mass of the spatial concentration profile for various time steps from $\Delta t_T = 120$ s to 5400 s, using the CBMOC, is shown in Figures 6(a)–(c), respectively for Cases 1, 2 and 3.

The results reveal (see figures) that the evolution of the phase error with time tends towards a limit curve with increasing values of the transport time step Δt_T, in all three cases. Each of these three limit curves stabilizes at a constant value of the phase error as time progresses, this value being negative in all three cases. The reason for it to become constant in time is that, in the wake of the wave, the flow becomes effectively uniform and steady. Therefore no additional tracking errors are generated, although any tracking error that had occurred before this stage remains. The fact that, for each case, this eventual tracking error seems to be almost independent of Δt_T, at least when the latter is large, is in accordance with the fact that the characteristic tracking process is based on the same flow data sampled at the same resolution, for all values of Δt_T. It is simply segmented in more or fewer steps depending on Δt_T.

However, the curves obtained with the smallest values of Δt_T, particularly in Cases 1 and 3, appear to be shifted upwards. This feature is of minor significance to the issue of characteristic tracking errors: it is explained by the fact that the use of smaller time steps implies the more frequent repetition of the process of interpolation at the foot of the characteristics. Hence there is the more frequent occurrence of (albeit small) interpolation errors as Δt_T reduces. These errors add up and thereby affect the location of the centre of mass of the concentration profile.[¶¶] It is worth reiterating that apart from the interpolation issue, the choice of Δt_T does not otherwise have any effect on the eventual phase error caused by the characteristic tracking process, because all the simulations are based on the same velocity field.

The most important observations to be made concern the magnitudes of the eventual tracking error obtained at the end of the simulation. In Case 1 (Figure 6(a)), it is approximately (−) 2.9 m (transport is predicted slower than it should). This is to be compared to the size of the discretization in space, $\Delta x = 100$ m, and to the distance travelled of almost 45 000 m. In Case 2 (Figure 6(b)), it has been reduced by 5% only, from (−) 2.9 m with $\Delta x = 100$ m to (−) 2.75 m with $\Delta x = 50$ m,

[¶¶] In these tests, the tracking error and this additional phase error counteract each other with various outcomes. For example, for $\Delta t_T = \Delta t_{CFD} = 120$ s, see Figure 6(a), the two errors fortuitously cancel each other out. However, this particular result is not representative and is not to be generalized.

DOI: 10.1002/fld

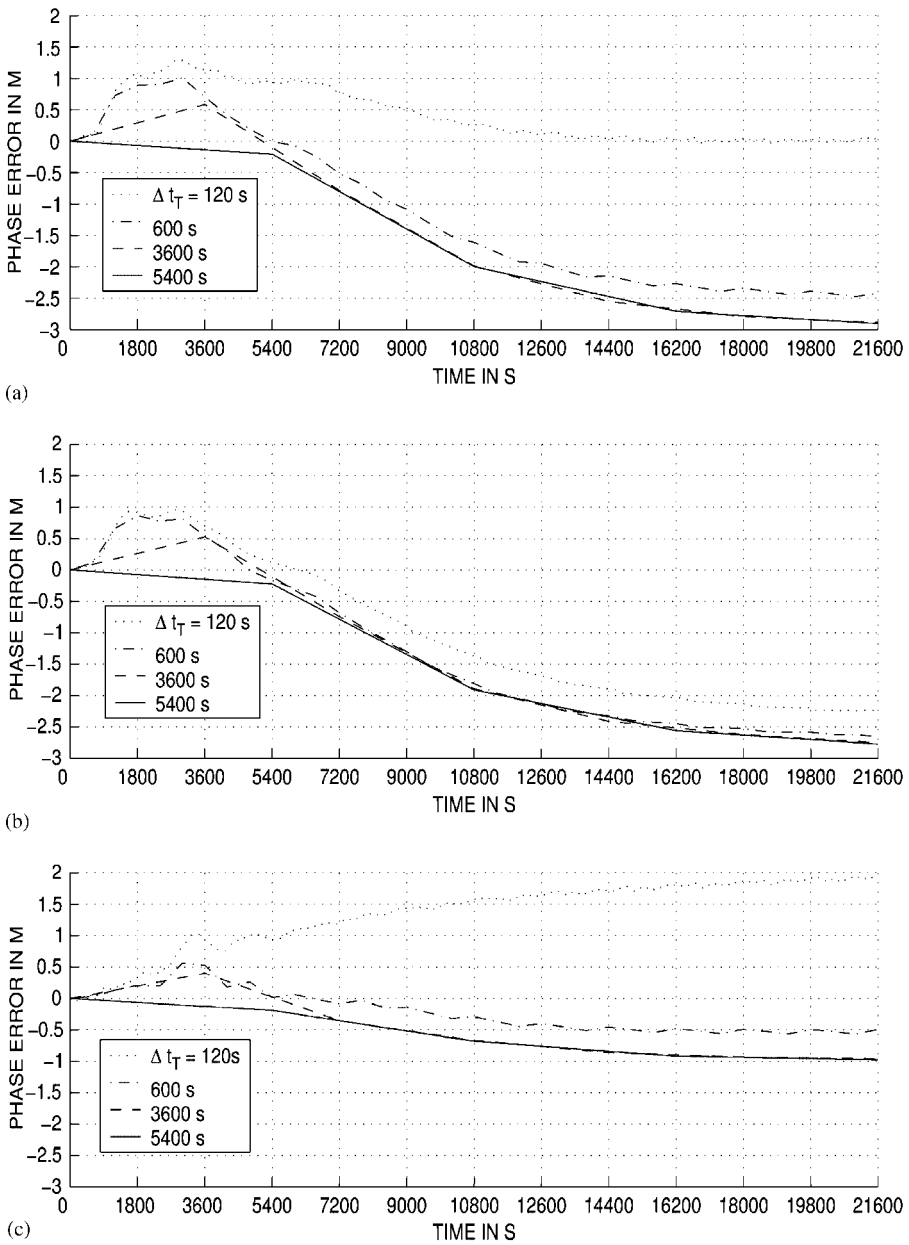

Figure 6. Evolution of the phase error at the centre of mass vs time, for the CBMOC results and with different solute transport time steps, for: (a) Case 1; (b) Case 2; and (c) Case 3.

DOI: 10.1002/fld

despite the better resolution in space in Case 2. This indicates that the non-uniformities (in space) caused by the nature of the flow are of a mild nature, hereby making the results only marginally sensitive to Δx. In Case 3 (Figure 6(c)), where $\Delta t_{\mathrm{CFD}} = 60$ s instead of 120 s, the phase error is strongly reduced, and stabilizes at less than $(-)$ 1 m, instead of $(-)$ 2.9 m in Case 1. This shows that reducing Δt_{CFD} is an efficient way to reduce the phase error occurring with the CBMOC.

The effect of the phase error on the errors experienced by the concentrations depends on the size and shape of the concentration profile: for a Gaussian profile with $\Sigma = 4$ ($\sigma = \Sigma \cdot \Delta x = 400$ m), and with the phase error of 2.9 m obtained in Case 1, the maximum relative error in the central part of the profile where $C \geqslant C_{\mathrm{peak}}/10$ is of the order of 1%, but this would be even smaller for larger values of Σ.

4.5. Discussion

The test case presented above corresponds to a very severe discharge increase from 10 to 50 $\mathrm{m^3\,s^{-1}}$ over 8 min, causing an increase of velocity from 1.43 to 2.14 $\mathrm{m\,s^{-1}}$. Yet tracing a characteristic line using the CBMOC through such a velocity field induced a small tracking error of less than 3 m. It should be reminded that under natural conditions where floods are caused by heavy precipitation, discharge increases in rivers occur over time scales significantly larger than a few minutes, resulting in milder velocity gradients than in the example, and, accordingly, smaller tracking errors. Even when some extreme circumstances (earthquakes, landslides, glacier outbursts, reservoir gate opening, dam breaks) do cause exceptional floods, these are highly unlikely to occur more than once over a short time scale. Therefore, any original tracking error should not be expected to grow during the remainder of any simulation.

Should modellers wish to reduce the errors to a minimum, an efficient way to do so consists in reducing Δt_{CFD}, the time step used in the modelling of the flow.

5. COMPUTATIONAL COST

As mentioned earlier, semi-Lagrangian transport schemes have the potential for requiring much shorter run times than Eulerian transport schemes, through the use of much larger time steps. However, each time step itself is expected to require more computational time, due to the computation of the characteristic lines and the interpolations at their feet. This must not offset the benefit of using longer time steps.

In order to verify this, measurements of computational time were undertaken in an example concerning a river 49 800 m long, divided into cells of length $\Delta x = 200$ m. The maximum value of the (unsteady) velocity was 0.65 $\mathrm{m\,s^{-1}}$, and the time step used in the flow model, Δt_{CFD}, was equal to 1000 s, corresponding to a maximum (flow) Courant number of 3.25. Solute transport (including *both* advection and dispersion) was simulated for a duration of $T = 72\,000$ s. Table III shows measured computation times for (1) the (Eulerian) SMART method [40] used with a (transport) Courant number close to 1/3, which is the maximum value permitted [41], and (2) the CBMOC method using cubic interpolation at the departure points, with increasingly large time steps. In both cases, dispersion was modelled using the Crank–Nicholson method for diffusion.

Table III shows that although the computation time per time step for the CBMOC did increase with increasing values of Δt_{T} (because characteristic lines are longer in this case), the total

DOI: 10.1002/fld

Table III. Measured computation times.

Scheme	Δt_T (s)	Cr	τ_A (s)	τ_D (s)	N	t (s)
SMART	100	0.325	0.1	0.2	720	216
CBMOC	1000	3.25	0.47	0.2	72	48.24
	4000	13	0.66	0.2	18	15.48
	9000	29.25	1.1	0.2	8	10.4
	12 000	39	1.28	0.2	6	8.88
	18 000	58.5	1.65	0.2	4	7.4
	24 000	78	2.14	0.2	3	7.02
	36 000	117	3.1	0.2	2	6.6

Δt_T, transport time step; Cr, (transport) Courant number; τ_A, computation time for advection, per time step; τ_D, computation time for diffusion, per time step; N, number of time steps; t, total computation time.

computation time decreased significantly, because of the smaller number of time steps to be computed. It was one order of magnitude smaller than with the Eulerian scheme for Cr of the order of 10, and about 30 times smaller for Cr of the order of 100. It must be emphasized that the above results were obtained without any specific optimization of the programming of characteristic tracking, that the cell-based approach for the characteristic lines would allow [7], hereby allowing even shorter computation times.

6. CONCLUSION

This article is concerned with the application of semi-Lagrangian methods to the numerical simulation of the 1D advection–dispersion equation in steady non-uniform or unsteady river flows, with a particular emphasis on the phase errors that occur during the process of tracking the characteristics.

A simple cell-based method of characteristics (CBMOC) assuming quasi-linear inter-node variation of velocity has been found to be subject to negligible tracking errors in a highly unsteady flow scenario comparable to that caused by a natural flood event. In non-uniform flows, these tracking errors are also unlikely to be significant in practical applications. Should they grow with distance in highly non-uniform flows featuring repeated velocity variations, an efficient way to reduce them consists of reducing the space step Δx, because the tracking errors have a second-order dependency on Δx. It should also be borne in mind, however, that it is unclear whether 1D representations of river hydrodynamics and the 1D advection–dispersion equation itself are adequate models of the physical processes in such flow cases. So that in practical applications, these uncertainties are probably no less a source of error than that associated with characteristic tracking.

It was found that in the semi-Lagrangian simulations, no limitation on the size of the (transport) time step arises because of tracking errors. This is due to the spatial resolution of the characteristic lines being independent of the time step used in the proposed CBMOC method.

Finally, a semi-Lagrangian model involving the CBMOC and the Crank–Nicholson method for diffusion has been shown to allow a very significant computation time saving (of at least 90% with Courant numbers of the order of 10) in the modelling of advection–dispersion, compared to an Eulerian method (and even more so at higher Courant numbers).

DOI: 10.1002/fld

REFERENCES

1. Martin JL, McCutcheon SC. *Hydrodynamics and Transport for Water Quality Modeling*. Lewis Publishers: Boca Raton, 1999.
2. Fischer HB, List EJ, Koh RCY, Imberger J, Brooks NH. *Mixing in Inland and Coastal Waters*. Academic Press: New York, 1979.
3. Rutherford JC. *River Mixing*. Wiley: Chichester, U.K., 1994.
4. Jensen JL, Lake LW, Corbett PWM, Goggin DJ. *Statistics for Petroleum Engineers and Geoscientists*. Elsevier Science: Amsterdam, The Netherlands, 2000.
5. Manson JR, Pender G, Wallis SG. Limitations of traditional finite volume discretisations for unsteady computational fluid dynamics. *AIAA Journal* 1996; **34**(5):1074–1076.
6. Wallis SG, Manson JR, Rafique S. Limitations of advection–dispersion calculations in rivers. In *Proceedings of the 28th IAHR Congress*, Graz, Austria, 21–27 August 1999.
7. Roache PJ. A flux-based method of characteristics. *International Journal for Numerical Methods in Fluids* 1992; **15**:1259–1275.
8. Staniforth A, Côté J. Semi-Lagrangian integration schemes for atmospheric models—a review. *Monthly Weather Review* 1991; **119**:2206–2223.
9. Oliveira A, Baptista AM. A comparison of integration and interpolation Eulerian–Lagrangian methods. *International Journal for Numerical Methods in Fluids* 1995; **21**:183–204.
10. Russell TF, Celia MA. An overview of research on Eulerian–Lagrangian localized adjoint methods (ELLAM). *Advances in Water Resources* 2002; **25**:1215–1231.
11. Manson JR, Wallis SG. Conservative semi-Lagrangian algorithm for pollutant transport in rivers. *Journal of Environmental Engineering* (ASCE) 1999; **125**(5):486–489.
12. Manson JR, Wallis SG. A conservative, semi-Lagrangian fate and transport model for fluvial systems: Part 1—theoretical development. *Water Research* 2000; **34**(15):3769–3777.
13. Wallis SG, Manson JR. Accurate numerical simulation of advection using large time steps. *International Journal for Numerical Methods in Fluids* 1997; **24**:127–139.
14. Fischer HB. The mechanics of dispersion in natural streams. *Journal of the Hydraulics Division* (ASCE) 1967; **93**:187–216.
15. Wallis SG, Manson JR. Methods for predicting dispersion coefficients in rivers. *Water Management*, *Proceedings of the Institution of Civil Engineers* 2004; **157**:131–141.
16. Abbott MB, Basco DR. *Computational Fluid Dynamics*: *an Introduction for Engineers*. Longman Scientific & Technical: Singapore, 1989.
17. Leonard BP. A stable and accurate convective modelling procedure based on quadratic upstream interpolation. *Computational Methods in Applied Mechanics and Engineering* 1979; **19**:59–98.
18. Courant R, Friedrichs KO, Lewy H. Über die partiellen differenzgleichungen der mathematischen physik. *Mathematische Annalen* 1928; **100**:32–74.
19. Leonard BP. Stability of explicit advection schemes. The balance point location rule. *International Journal for Numerical Methods in Fluids* 2002; **38**:471–514.
20. Al-Lawatia M, Sharpley RC, Wang H. Second-order characteristic methods for advection–diffusion equations and comparison to other schemes. *Advances in Water Resources* 1999; **22**(7):741–768.
21. Bonaventura L. A second order, semi-Lagrangian scheme with accurate approximation of trajectories. In *Proceedings of the 10th International Conference on Numerical Methods for Laminar and Turbulent Flow*, Taylor C, Cross J (eds). Pineridge Press: Swansea, U.K., 1997.
22. Croucher AE, O'Sullivan MJ. Numerical methods for contaminant transport in rivers and estuaries. *Computers and Fluids* 1998; **27**(8):861–878.
23. Karpik SR, Crockett SR. Semi-Lagrangian algorithm for two-dimensional advection–diffusion equation on curvilinear coordinate meshes. *Journal of Hydraulic Engineering* (ASCE) 1997; **123**(5):389–401.
24. Malevsky AV, Thomas SJ. Parallel algorithms for semi-Lagrangian advection. *International Journal for Numerical Methods in Fluids* 1997; **25**:455–473.
25. Oliveira A, Baptista AM. On the role of tracking on Eulerian–Lagrangian solutions of the transport equation. *Advances in Water Resources* 1998; **21**:539–554.
26. Roache PJ. *Computational Fluid Dynamics*. Hermosa: Albuquerque, 1976.
27. Wang HQ, Lacroix M. Interpolation techniques applied to the Eulerian–Lagrangian solution of the convection–dispersion equation in natural coordinates. *Computers and Geosciences* 1997; **23**(6):677–688.

DOI: 10.1002/fld

28. Ruan F, McLaughlin D. An investigation of Eulerian–Lagrangian methods for solving heterogeneous advection-dominated transport problems. *Water Resources Research* 1999; **35**(8):2359–2373.
29. Schohl GA, Holly FM. Cubic-spline interpolation in Lagrangian advection computation. *Journal of Hydraulic Engineering* (ASCE) 1991; **117**(2):248–253.
30. Zoppou C, Roberts S, Renka RJ. Exponential spline interpolation in characteristic based scheme for solving the advective-diffusion equation. *International Journal for Numerical Methods in Fluids* 2000; **33**:429–452.
31. Neuman SP. Adaptive Eulerian–Lagrangian finite element method for advection–dispersion. *International Journal for Numerical Methods in Engineering* 1984; **20**:321–337.
32. Néelz S. Semi-Lagrangian methods applied to pollutant transport modelling in rivers. *Ph.D. Dissertation*, Heriot-Watt University, Edinburgh, U.K., 2003.
33. Neuman SP. A Eulerian–Lagrangian numerical scheme for the dispersion-convection equation using conjugate space-time grids. *Journal of Computational Physics* 1981; **41**:270–294.
34. Oliveira A, Fortunato AB. Toward an oscillation-free, mass conservative, Eulerian–Lagrangian transport model. *Journal of Computational Physics* 2002; **183**:142–164.
35. Burguete J, Garcia-Navarro P. Semi-Lagrangian conservative schemes *versus* Eulerian schemes to solve advection in river flow transport. In *Proceedings of the Fifth International Conference on Hydroinformatics*, Cluckie ID, Han D, Davis JP, Heslop S (eds). Cardiff, U.K., 2002; 180–185.
36. Zoppou C, Roberts S. Conservative semi-Lagrangian algorithm for pollutant transport in rivers. *Journal of Environmental Engineering* (ASCE) 2000; **126**(9):878–879.
37. Chatwin PC. Presentation of longitudinal dispersion data. *Journal of the Hydraulics Division* (ASCE) 1980; **106**:71–83.
38. Nordin CF, Troutman BM. Longitudinal dispersion in rivers: the persistence of skewness in observed data. *Water Resources Research* 1980; **16**:123–128.
39. Sobey RJ. Evaluation of numerical models of flood and tide propagation in channels. *Journal of Hydraulic Engineering* (ASCE) 2001; **127**(10):805–824.
40. Gaskell PH, Lau KC. Curvature-compensated convective transport: SMART, a new boundedness-preserving transport algorithm. *International Journal for Numerical Methods in Fluids* 1988; **93**:617–641.
41. Halcrow, Wallingford HR. *ISIS Quality User Manual*, 1999.

DOI: 10.1002/fld